UC Davis

UC Davis Previously Published Works

Title

BASS: Safe Deep Tissue Optical Sensing for Wearable Embedded Systems

Permalink

https://escholarship.org/uc/item/3ws2r1rm

Journal

ACM Transactions on Embedded Computing Systems, 22(5s)

ISSN

1539-9087

Authors

Vali, Kourosh

Vafi, Ata

Kasap, Begum

et al.

Publication Date

2023-10-31

DOI

10.1145/3607916

Peer reviewed

BASS: Safe Deep Tissue Optical Sensing for Wearable Embedded Systems

KOUROSH VALI,

University of California, Davis, Electrical and Computer Engineering Department, USA;

ATA VAFI,

University of California, Davis, Electrical and Computer Engineering Department, USA;

BEGUM KASAP,

University of California, Davis, Electrical and Computer Engineering Department, USA;

SOHEIL GHIASI

University of California, Davis, Electrical and Computer Engineering Department, USA.

Abstract

In wearable optical sensing applications whose target tissue is not superficial, such as deep tissue oximetry, the task of embedded system design has to strike a balance between two competing factors. On one hand, the sensing task is assisted by increasing the radiated energy into the body, which in turn, improves the signal-to-noise ratio (SNR) of the deep tissue at the sensor. On the other hand, patient safety consideration imposes a constraint on the amount of radiated energy into the body. In this paper, we study the trade-offs between the two factors by exploring the design space of the light source activation pulse.

Furthermore, we propose BASS, an algorithm that leverages the activation pulse design space exploration, which further optimizes deep tissue SNR via spectral averaging, while ensuring the radiated energy into the body meets a safe upper bound. The effectiveness of the proposed technique is demonstrated via analytical derivations, simulations, and *in vivo* measurements in both pregnant sheep models and human subjects.

Additional Key Words and Phrases:

medical cyber-physical systems; design space exploration; multi-objective optimization; wearable embedded systems; deep tissue optical sensing; internet of medical things

kvali@ucdavis.edu .

1   INTRODUCTION

A growing number of applications involve deep tissue optical sensing using wearable-grade electronics. In such systems, light generated by emitters, such as light-emitting diodes (LEDs), is radiated into the body toward the tissue of interest. The radiated light diffuses into the tissue bed, and a small fraction of the diffused light is non-invasively detected by light sensors in the wearable system. The detected light may have propagated through multiple tissue layers, including a deep tissue of interest, whose chemical composition regulates light attributes, such as its intensity, thereby enabling the system to non-invasively sense specific tissue properties [34].

Human tissue is a highly scattering medium for light. As a result, the amount of light energy that is received by a light detector on the subject's skin is far smaller than the radiated energy in the body. This makes the task of embedded system design challenging, as it needs to faithfully sense and capture very weak signals that are due to the deep tissue of interest.

An illustrative application of deep tissue sensing is non-invasive fetal oximetry, in which the goal of the wearable system is to perform pulse oximetry on an *in utero* fetus from outside of the maternal abdomen [32, 36]. A high-level sketch of this application is shown in Figure 1. The red *banana pattern* highlights in the figure illustrate the average path that is traveled from the light emitters to the detectors by the majority of sensed light photons [6, 21].

The signal detected by the photo-detectors is essentially the photoplethysmogram (PPG) signal, which is obtained optically. It records the variations in light absorption caused by changes in blood volume. The PPG signal is commonly used in pulse oximetry applications, where the goal is to measure a patient's blood oxygen saturation (SpO_2) using a wearable device typically attached to the finger. Pulse oximetry underpinnings rely on the principle that oxygenated and deoxygenated blood absorb light differently, depending on the wavelength of the light source [13]. By illuminating the tissue with two light sources of different wavelengths and measuring the changes in their respective light absorption, it is possible to establish a correlation between the change in light absorption and the patient's SpO_2.

The light signal detected by a sensor placed farther from the light source contains more information about the deep tissue, however, its detection is potentially challenging due to high attenuation over the longer path [1, 10]. A naive approach to solve this problem is to increase the amount of radiated energy into the body, to proportionally increase the detected signal. This approach would not offer a practical solution, as safety considerations limit the amount of radiated energy into the body [5].

The question then arises of whether the wearable embedded system can be designed to optimize the quality of the sensed light signal under a given constraint on the emitted optical energy. This paper addresses this very problem via two methods that complement each other on the light emission and light detection side of the system.

Specifically, we first explore the design space of the pulses, characterized by the two LED forward current (I_{FD}) and pulse duty cycle (d) parameters, that are used to activate the light

emitter, and derive pulse activation functions that lead to improved SNR at the detector. Subsequently, we develop BASS, an application-specific signal averaging technique, which leverages scaled spectral copies of the signal to improve SNR. Unlike conventional time-domain signal averaging methods [27], which find limited application in sensing dynamic systems, BASS utilizes scaled replicas of the signal spectrum that are concurrently sensed.

The objective of this paper is to propose a technique that can alleviate the burden on hardware design. The fundamental design of an optimized embedded system for deep tissue sensing must take power efficiency into account and at the same time report reliable readings.

The contributions of this paper are as follows:

- In the context of wearable light-based sensing, we identify, formulate and investigate the optimization of the light source activation signal to achieve maximum signal-to-noise ratio (SNR) under a critically-important given radiated energy budget.

- We propose a novel algorithm called BASS, which utilizes multiple scaled replicas of the tissue signal to improve the SNR of the deep tissue signal to improve the performance of the sensing modality.

- We provide analytical derivations and simulation results to support the proposed techniques' effectiveness. Furthermore, we implement the proposed algorithms in an existing deep tissue sensing system prototype. We report experimental results based on measurements collected from benchtop tissue phantoms, animal models as well as human subjects.

2 RELATED WORKS

The main issue with deep tissue sensing is that the signal peak is very close to the noise floor and there have been many attempts in finding means to split the tissue signal from the noise floor. One application of deep tissue sensing is in fetal oximetry which we alluded to before. In one of our previous works, we explored the use of particle filters to estimate the fetal signal more accurately which was tested on pregnant ewe [19]. In another previous work, we looked into using adaptive noise cancellation techniques to suppress the maternal signal in the mixed signal detected in this deep tissue sensing modality as seen in [7] which was also explored in related works such as [2, 3]. In another work, the objective was designing algorithms to track the fetal signal amidst noise, utilizing prior information about the signal of interest [15]. In addition, spatial information fusion from multiple light detectors was used to enhance the accuracy of deep tissue oximetry utilizing LED light sources within the red to near-infrared (NIR) wavelength ranges as explained in [9, 17]. The effect of measurement depth in oximetry was also explored in related work [24] using spatially resolved near-infrared spectroscopy.

A non-invasive deep tissue optical sensing system was proposed in previous work [10], which involves the use of a NIR light source operating at approximately $850nm$ within a high-power LED package. This particular setup is known as the Transabdominal Fetal

Pulse Oximetry (TFO) system, which is specifically designed to extract fetal information from deep within the maternal abdomen non-invasively. To achieve this objective, improving the SNR of the fetal photoplethysmogram (PPG) signal in this application is crucial while minimizing exposure to the maternal skin. The improvements discussed in this paper involve the implementation of a novel and modified TFO system.

In a different study, researchers explored an invasive system for monitoring deep-tissue oxygen saturation using a wireless implant. This method utilizes LEDs for sensing oxygen saturation and allows for implantation within deep tissue, powered by an ultrasound linkage [28]. Additionally, efforts have been made to develop minimally invasive solutions. In one approach described in [22], an array of microneedle waveguides is utilized on a patch attached to the skin. These waveguides enhance the penetration depth of photons emitted by the LEDs, consequently improving the performance of deep tissue sensing.

In addition, different sensing modalities have been explored for similar deep tissue sensing applications. For instance, bioimpedance spectroscopy is used to investigate the tissue under contact points [16, 30] but would require more electronics attached to the skin and might not be suitable for wearable power-efficient embedded systems.

In various RF applications, shaping the input signal is standard practice. This technique is commonly used in digital communication to reduce signal distortion within the communication channel [20]. However, in optical sensing, this technique is employed to maximize the performance of LED emitters. One key difference is that the generated optical signal always has a non-negative amplitude due to the non-negativity of the LED current. In contrast, in RF applications, the input waveform is generated by the transmitter and applied to an antenna, which can have positive or negative amplitudes. Once the waveform reaches the target, it interacts with it causing modulation, and a portion of the signal is reflected back toward the receiver. Additionally, the amount of RF radiated power from the antenna is not exactly proportional to the generated signal power in the transmitter [26]. This necessitates a different optimization problem, which distinguishes it from optical sensing applications.

Previous studies have demonstrated that utilizing signal averaging methods can improve the SNR performance of sensing modalities. Traditional time-domain signal averaging techniques, such as those mentioned in [4, 27] rely on taking multiple measurements to reduce the impact of uncorrelated noise. However, in the case of the sensing modality proposed in this paper which is designed for dynamic systems, newly acquired data at different times may not exhibit a strong correlation with previous data. Therefore, in the proposed algorithm, signal averaging is applied to multiple harmonics within one frame of acquired PPG data as will be discussed in Section 5.

In RF applications, the measurement bandwidth is usually high, and accessing higher harmonics of the carrier signal is typically not feasible. Consequently, the wideband application requires capturing these higher harmonics, which increases the cost, the complexity of the hardware, and the power consumption [33]. In contrast, in optical sensing applications, the operation frequency is generally much lower, and accessing higher harmonics is not challenging when using a typical Analog-to-Digital Converter (ADC).

Therefore the algorithm proposed in this paper can be applied within the software domain which is favorable.

The proposed method in this paper is expected to work on any deep tissue sensing applications as long as LEDs are used as the light source. Essentially, LEDs are non-ionizing light sources that pose minimal risks to the tissue but require some additional considerations to achieve desirable performance. Previous works have looked into lowering the duty cycle of the input signal in an optical sensing application. Authors in [11, 29] have looked into lowering the duty cycle of a pulse oximetry system in favor of lowering the power consumption of the system which proved to be effective. However, it is pivotal to note that these works were studied on single-body patients and the target was not a deep tissue. So they could achieve desired performance with a low current by decreasing the duty cycle which is a challenge that will be discussed thoroughly in Section 4.2.

3 BACKGROUND

3.1 Safety Overview

The power of the reflected received signal from the deep tissue is proportional to the intensity of the emitted light from the light source. The higher the emitted light power, the higher the reflected received signal power from the deep tissue will be. However, the increase in the light source power rises the tissue temperature, which raises safety concerns for the patient.

In the case of human studies, the maximum permissible transmitted optical power is set by safety regulations. Complying with these standards consequently imposes a limit on the maximum penetration depth of the optical signal. Given this situation, the reflection from the deep tissue will be so small that it can be buried under the system's noise. As a result, the ever-lasting challenge of deep tissue sensing is the extraction of the reflected signal from the deep tissue of interest, considering the limitation on the maximum transmitted optical power.

The safety regulations mentioned earlier are defined by IEC 60601-2-57, a Recognized Consensus Standard approved by the U.S. Food and Drug Administration (FDA) [5]. These regulations apply to commercial products that utilize non-ionizing radiation sources, similar to the system employed in this paper, which motivates the problem at hand. Adhering to this standard is crucial as it mandates that the radiance levels emitted by the system remain below the thresholds for optical signals projected onto the body, ensuring the system's compliance for commercial and clinical purposes.

Throughout this paper, the average optical power generated by the light source (P_E) over the measurement capture time is considered a parameter that must be restricted. The findings are applicable and remain valid for any permitted threshold on P_E, thus ensuring the generalizability of the results. The effect of instantaneous generated optical power which arguably has adverse effects on the skin is not ignored in this paper despite having a pulse with a very short duration.

3.2 Optical Power for an LED

In this work, we utilize a non-ionizing light source to detect a signal buried in deep tissue inside the body. Specifically, in this paper, we investigate the use of LEDs for sensing, which are incoherent light sources and generally safer to use on human skin. As explained above, LEDs have more relaxed safety concerns compared to using lasers as the light source.

In this paper, we assume a linear relationship between the emitted optical power from the light source and the LED forward current (I_{FD}). Additionally, we assume that all the power generated by the light source is radiated toward the body. For an LED activated using a pulse signal at a fixed frequency of f_c, the average power of the emitted light (P_E) from the light source can be calculated using Equation 1. Here, $P(I_{FD})$ represents the peak emitted optical power from the LED, which can be obtained from the LED's datasheet for a fixed I_{FD}. T_p denotes the pulse duration, and T represents the period of the pulse signal. The ratio of T_p/T can also be denoted as d, which refers to the duty cycle of the activation pulse.

$$P_E = P(I_{FD})\frac{T_p}{T} = P(I_{FD})d$$

(1)

This indicates that the average power of emitted light is proportional to the duty cycle at I_{FD}, so if the duty cycle is decreased, effectively the light source power, and hence heat on the skin is decreased and vice versa.

Later we discuss how the LED activation signal has a direct effect on the optical power limitation then explain the trade-offs in optimizing the system's performance while staying below a certain optical power budget.

3.3 Synchronous Detection

$x(t)$ is the baseband signal that contains a signal of interest from the deep tissue that is aimed to be detected using this sensing modality. To detect this signal, the principles of synchronous detection as discussed in detail in [12] is utilized, where a light source is pulsated using an activation signal $\Pi(t)$ with the frequency of f_c which modulates the $x(t)$ to higher frequencies to achieve better SNR performance. By pulsating the light source using $\Pi(t)$ and capturing the reflected light from the body, inherently, $x(t)$ will be "modulated" to a higher frequency, as shown in Figure 2a. Here it is assumed that the signal of interest from deep tissue is a physiological signal with a frequency of f_{BB} limited to a few Hertz with the requirement of $f_c \gg f_{BB}$.

Figure 2a illustrates that after pulsating the LED with a periodic signal, $x(t)$ will be modulated to harmonics of f_c in the PPG signal received at the optical detector placed at a certain distance from the LED. The PPG signal is heavily attenuated as it has to traverse through and back from multiple shallower tissues as well as the deep tissue of interest. If we assume the tissue response to the LED is linear throughout all harmonics, we can express the PPG signal as such assuming that $\Pi(t)$ is a periodic even signal:

$$ppg\Big(t\Big) = Lx\Big(t\Big) \cdot \Pi\Big(t\Big)$$
$$= L \sum_{i} x\Big(t\Big) \cdot a_i cos(i\omega_c t)$$

(2)

In Equation 2, L is a constant comprised of multiple coefficients including but not limited to the tissue loss, the responsivity of the LED to the driver current, the responsivity of the detector to the received light, the area of the detector, and the gain of the data acquisition system. Here, $x(t)$ is the deep tissue signal, and $\Pi(t)$ is the driving signal of the light source. In this paper, we assume that L remains constant across different frequencies, as well as across various amplitudes and shapes of $\Pi(t)$.

Next, the PPG signal is sampled using a data acquisition system with a sampling rate of F_s assuming that the bandwidth of the data acquisition system is unlimited. The optical detector front-end and data acquisition pipeline will induce a noise added to the modulated signal. It is assumed this additive noise is a White Gaussian Noise (WGN) with the distribution of $N(0, \sigma_N^2)$ and only affects the amplitude of the PPG signal.

Finally, as outlined in Figure 2b, the noisy tissue signal $y_1(t)$ can be extracted from the fundamental frequency of the detected PPG signal. The sampled PPG signal is passed from a bandpass filter (BPF) centered at the fundamental frequency f_c and then mixed with a sinusoidal signal with the frequency of f_c which has the same phase as $\Pi(t)$, followed by a final lowpass filter (LPF) to ensure that the outcome signal is band-limited to f_{BB}. Here we "demodulate" the signal from f_c back to the baseband.

4   LED ACTIVATION SIGNAL

Knowing the underpinnings of synchronous detection, it's crucial to point out that the LED activation signal $\Pi(t)$ has an essential role in achieving optimum performance while maintaining the safety requirements of the application. The noisy tissue signal, which is extracted from the fundamental harmonic (f_c) of the PPG signal, can be represented as $y_1(t) = s_1(t) + n_1(t)$, where $s_1(t)$ denotes the tissue signal modulated at f_c in the PPG signal, and $n_1(t)$ is the WGN of the data acquisition system present around f_c as seen in Figure 2b. Here $s_1(t)$ is uncorrelated to noise ($E[s_1(t - \tau)n_1(t)] = 0, \forall t, \tau$). SNR_1 is defined around f_c of the detected PPG signal formulated in Equation 3.

$$SNR_1 = \frac{\overline{s_1^2(t)}}{E[n_1^2(t)]} = \frac{S_1}{N_1}$$

(3)

Here, the power of the tissue signal S_1 is the average sum of squares for all the samples in $s_1(t)$, and N_1 is the expected noise power at around f_c. The LED activation signal $\Pi(t)$ will be

converted to an optical signal by the LED which in turn assuming that the tissue responds linearly to the input optical signal, will affect the detected PPG signal from the deep tissue. This means that S_1 is directly affected by the shape of the input signal $\Pi(t)$.

4.1 Optimal LED Activation Signal

The primary objective is to determine the optimal periodic signal for LED activation, ensuring the best SNR_1 performance while keeping the average emitted power by the LED (P_E) below a certain threshold. For the general case, it is assumed the LED activation signal can have infinite bandwidth. So $\Pi(t)$ can have any shape or format as long as it's a periodic signal with a period of $T = 1/f_c$ and has a non-negative value at each sample with an average below a certain threshold since the activation signal of the LED can not be negative. Furthermore, the average of $\Pi(t)$ is bounded in the conditions because it will correlate with the average emitted power of the optical light on which the optical power budget is enforced $\left(P_E \propto \overline{\Pi(t)}\right)$.

Assuming $\Pi(t)$ is an even periodic function of t, which only has cosine coefficients in $\Pi(t)$ Fourier series $\sum a_i \cos(2i\pi t/T)$, in order to maximize S_1, one can maximize the first cosine coefficient in $\Pi(t)$ Fourier series (a_1). Assuming a sampling rate $F_s \gg 2f_c$, the signals will be sampled with sampling period $T_s = 1/F_s$. In this case, we have $\Pi[n] = \Pi(nT_s)$ where the sampled Π has $N = T/T_s$ samples in a period ($\Pi[n+N] = \Pi[n]$). This will translate to the following optimization problem in the discrete domain which is a linear programming problem:

$$\max \quad \sum_{n=0}^{N-1} \Pi\left[n\right]\cos\left(\frac{2n\pi}{N}\right)$$
$$\text{s.t.} \quad \Pi[n] \geq 0, \quad n = 0,1,\ldots,N-1$$
$$\sum_{n=0}^{N-1} \Pi\left[n\right] \leq \Gamma.$$

Here Γ is selected such that the average emitted optical power P_E is within the specifications of the application.

Theorem 4.1. *The solution to this problem in the discrete domain is a periodic Kronecker delta function that has a positive value when $\cos(2n\pi/N) = 1$ and zero for the rest. This Value can be Γ to satisfy the requirements. As a result, Π' is the feasible and optimal solution to the problem, and within one period:*

$$\Pi' = \begin{cases} \Gamma & if \;\; n = 0 \\ 0 & if \;\; n = 1,\ldots,N-1 \end{cases}$$

(4)

which maximizes the objective function at $\sum_n \Pi'[n]\cos(2n\pi/N) = \Gamma$.

Proof. Suppose Π' is not optimal. Then, $\exists \Pi^\star$, a feasible and optimal solution to the linear programming problem above, such that $\Pi^\star$ maximizes $\sum_n \Pi[n]\cos(2n\pi/N)$. Since Π' is not optimal:

$$
\sum_{n=0}^{N-1} \Pi^\star\Big[\Big|n\Big|\Big] \geq \sum_{n=0}^{N-1} \Pi^\star\Big[\Big|n\Big|\cos\Big(\frac{2n\pi}{N}\Big), \text{ as } \Pi^\star \geq 0
$$

$$
\sum_{n=0}^{N-1} \Pi^\star\Big[\Big|n\Big|\cos\Big(\frac{2n\pi}{N}\Big) > \sum_{n=0}^{N-1} \Pi'\Big[\Big|n\Big|\cos\Big(\frac{2n\pi}{N}\Big)
$$

$$
\Rightarrow \sum_{n=0}^{N-1} \Pi^\star[n] > \Gamma,
$$

An optimal solution has to be feasible as well. $\Pi^\star$ is a feasible solution $\Leftrightarrow \sum_n \Pi^\star[n] \leq \Gamma \,\&\, \Pi^\star \geq 0$. Here $\Pi^\star$ does not satisfy the first feasibility requirements so it cannot be an optimal solution.

So $\Pi'[n] = \Gamma\delta[n \pm kN]$ where $k = 0,1,2,\dots$ is the optimal periodic function to use as the LED activation signal which maximizes S_1 and adheres to limits enforced over P_E.

Realistically, in the time domain, a signal with a high value at a specific time and zero for the rest has infinite bandwidth and even if we use it as the activation signal of conventional high-power LEDs, the emitted optical signal has limited bandwidth. Thus, we settle for a pulse train instead with a short duty cycle but high amplitude to drive the LED.

4.2 SNR vs Duty Cycle of the LED Activation Pulse

Henceforth $\Pi(t)$ will be denoted as the LED activation "pulse", which is a periodic pulse train with a duty cycle of d, frequency of f_c, and current amplitude of A expressed as $\Pi(t) = Ad + \sum_{i=1}^{\infty} a_i\cos(i\omega_c t)$. Here $a_i = 2Ad\,\mathrm{sinc}(id)$ where $\mathrm{sinc}(id) = \sin(\pi id)/(\pi id)$. As indicated in Equation 1, the peak emitted optical power from the LED is proportional to the LED forward current (I_{FD}) which is defacto the amplitude of the pulse train (A). In addition, here we assume that tweaking P and d, will not affect the system noise. The extracted tissue signal from f_c in the detected PPG signal is $S_1 = \overline{s_1^2(t)} = L^2 A^2 d^2 \mathrm{sinc}^2(d)\overline{x^2(t)}$ if the LED activation pulse has a duty cycle of d and pulse amplitude of A, assuming constant loss term L.

Yet, we have to make sure the average emitted optical power complies with the power budget. P_E must be contained which translates to keeping the average of activation pulse ($\overline{\Pi}$) constant, and as such $\overline{\Pi} = A_1 d_1 = A_2 d_2$. Thus the SNR improvements for two design points with different duty cycles of d_1 and d_2 but the same P_E will be:

$$
\frac{\mathrm{SNR}_1(d_2)}{\mathrm{SNR}_1(d_1)} = \frac{S_1(d_2)}{S_1(d_1)} = \frac{A_2^2 d_2^2 \mathrm{sinc}^2(d_2)}{A_1^2 d_1^2 \mathrm{sinc}^2(d_1)} = \frac{\mathrm{sinc}^2(d_2)}{\mathrm{sinc}^2(d_1)}
$$

(5)

Considering the SNR of the extracted tissue signal from f_c(SNR$_1$) after activating an LED with a pulse train with $d = 50\%$ and a period of $1/f_c$ as the baseline, the SNR improvement for various duty cycles while maintaining constant P_E is expected to follow Figure 3 with theoretical SNR improvement of ~$3.89dB$ for activating the LED with $d = 5\%$ and $10\times$ higher amplitude compared to $d = 50\%$.

5 SELECTIVE SPECTRAL AVERAGING

We propose BASS (Band Averaged Sensing Scheme), which employs scaled copies of the tissue signal spectrum that are simultaneously captured. Essentially by utilizing the fact that a pulse train has harmonics at not just the fundamental frequency but also integer multiples of the fundamental frequency in the frequency spectrum. As mentioned in Section 2, the technique discussed here operates on a single data frame collected.

This algorithm calculates an averaged extracted tissue signal which was initially modulated to the harmonics of the light carrier (ifc) by spectrum band averaging to reduce the noise floor of the tissue signal. As indicated before, it is assumed that the tissue has a linear response to the LED activation pulse which translates into the linear scaling of all the harmonics in the detected PPG signal.

5.1 Proposed Algorithm

Harmonic content M: Assuming that the data acquisition system has unlimited bandwidth, M denotes the amount of Harmonic content in the average extracted tissue signal. This indicates that the tissue signal copies are extracted from the first M harmonics of the PPG signal and selected to average.

In Figure 4, the high-level process of the BASS algorithm is depicted where the PPG signal from the light detector, which carries the tissue information modulated over all harmonics of the LED signal, is filtered around each harmonic if_c where f_c is the fundamental frequency of the LED activation signal and $i = 1,2\ldots M$ and brought back to the baseband by employing synchronous detection principles. Here slightly more advanced technique than the conventional synchronous detection method which was demonstrated in Figure 2b is utilized. After the detected PPG signal is passed from band-pass filter (BPF) banks centered at each harmonic (if_c), each output is mixed with a generated sine wave with the frequency of if_c and phase-synced to each signal with a phase-locked loop (PLL) which will be called the In-Phase component (I). Here the concept of I/Q demodulation is utilized where in addition to the In-Phase component, the phase-synced sine wave is shifted by 90° and mixed again with the output of each BPF, and the output signal will be denoted as the Quadrature component (Q) [20]. Finally, the magnitude of the mixed signal which is the root sum of squares of I and Q components is passed from LPF banks, all with the same cutoff frequency of f_{BB}, to extract the demodulated tissue signal from the M harmonics, as seen in Figure 4.

However, as mentioned before the extracted tissue signal from this algorithm is noisy. Here, $y_{\text{avg}}(t) = \frac{1}{M}\sum_{i=1}^{M} y_i(t)$, where $y_i(t)$ is the noisy extracted tissue signal from each harmonic of the fundamental frequency of the detected PPG signal. Here, the noisy extracted signal is $y_i(t) = s_i(t) + n_i(t)$, where $s_i(t)$ is the copy of the tissue signal which was modulated to if_c and $n_i(t)$ is WGN present around the ith harmonic. The copies of tissue signal $s_i(t)$ are uncorrelated to the noise around the corresponding harmonic ($E[s_i(t-\tau)n_i(t)] = 0, \forall t, \tau$).

SNR_{avg} is defined to measure the signal-to-noise ratio of the average tissue signal $y_{\text{avg}}(t)$ calculated from the BASS algorithm and formulated in Equation 6.

$$\text{SNR}_{avg} = \frac{S_{avg}}{N_{avg}} = \frac{\frac{1}{M^2}\overline{\left(\sum_{i=1}^{M} s_i(t)\right)^2}}{\frac{1}{M^2}E\left[\left(\sum_{i=1}^{M} n_i(t)\right)^2\right]} = \frac{\overline{\left(\sum_{i=1}^{M} s_i(t)\right)^2}}{E\left[\left(\sum_{i=1}^{M} n_i(t)\right)^2\right]}$$

(6)

In Equation 6, S_{avg} is the average power of M tissue signal copies $s_i(t)$ modulated at $if_c, i = 1, \ldots, M$, and N_{avg} is the average power of noise $n_i(t)$ at corresponding harmonics. It is assumed that the WGN of the data acquisition system is stochastic throughout the spectrum, which means the noise floor in all harmonics is the same $N_1 = E[n_1^2(t)] = \cdots = E[n_M^2(t)]$. By averaging the noise from the first M harmonics, N_{avg} will be N_1/M assuming that noises around each harmonic are uncorrelated with each other ($E[n_i(t-\tau)n_j(t)] = 0, i \neq j, \forall t, \tau$).

A pulse train is used as the LED activation signal having components at integer multiples of f_c in the frequency spectrum, which means the same baseband signal will be modulated to all the above harmonics, per modulation theorem, [25]. So the corresponding tissue signal copies at each of these harmonics ($s_i(t)$) are actually correlated with each other.

So, it is relatively safe to assume the extracted tissue signal from the ith harmonic of the PPG signal is a scaled replica of the tissue signal copy from the fundamental frequency of the PPG signal where $s_i(t) = \alpha_i s_1(t)$ for the same duty cycle.

In Equation 7, α_i^2 represents the ratio of the tissue signal power extracted from the i-th harmonic compared to the extracted tissue signal power from the fundamental. This ratio can be calculated based on the relationship between $s_1(t)$ and $s_i(t)$, where $s_1(t) \propto a_1 x(t)$ and $s_i(t) \propto a_i x(t)$.

$$\implies \frac{S_i}{S_1} = \frac{\overline{s_i^2(t)}}{\overline{s_1^2(t)}} = \frac{a_i^2}{a_1^2} = \frac{sinc^2(id)}{sinc^2(d)} = \alpha_i^2$$

(7)

As seen in Equation 6, the term $\overline{\left(\sum_i s_i(t)\right)^2}$ can be replaced with $\sum_i \alpha_i^2 \overline{s_i^2(t)}$ due to the correlated nature of the tissue signal copies around harmonics. Therefore, Equation 6 can

be reformatted to Equation 8 for calculating the SNR of the first M extracted tissue signals averaged with duty cycle of d:

$$\mathrm{SNR}_{avg}\left(d, M\right) = \frac{\overline{\left(\sum_{i=1}^{M} s_i(t)\right)^2}}{E\left[\left(\sum_{i=1}^{M} n_i(t)\right)^2\right]} = \frac{\left(\sum_{i=1}^{M} \alpha_i\right)^2}{M} \cdot \frac{S_1}{N_1}$$

$$= \frac{\left(\sum_{i=1}^{M} \alpha_i\right)^2}{M}\mathrm{SNR}_1$$

(8)

A limitation of this method is that even though the noise floor is reduced, the averaged extracted signal from different harmonics will have lower power compared to the extracted tissue signal from the fundamental. This is evident by analyzing the Fourier series of the LED activation pulse, where the magnitude of the Fourier coefficients decreases as the harmonic number increases. However, if the focus is shifted to pulse trains with a lower duty cycle (less than 10% duty cycle), the Fourier coefficients diminish less, resulting in similar magnitudes. This leads to tissue signal copies around the harmonics having more comparable amplitudes.

5.2 BASS in a Simulated Setup

The signal from the deep tissue was simulated as a sinusoidal wave with a frequency of $2.5\,Hz$ and the activation pulse as a pulse train with a frequency of f_c. In this simulated setup, the average emitted optical power P_E was kept constant while varying the LED duty cycle. We considered the baseline case with a duty cycle of $d = 50\%$ and an LED activation pulse amplitude of $A = 1$. For other duty cycles, we adjusted the pulse amplitude by increasing it by $0.5/A$ to maintain a constant average activation pulse $(\overline{\Pi})$ as explained previously. The PPG signal was generated by mixing the modeled tissue signal with the modeled optical signal from the LED activated by a pulse train. This PPG signal was then sampled with a frequency of Fs. In these simulations, the WGN noise was stochastic and randomly generated with a predetermined variance of σ_N^2 and then was added as an amplitude noise to the sampled PPG signal.

Figure 5 displays the Power Spectral Density (PSD) of the average extracted tissue signal in two examples. In Figure 5a, the SNR of the extracted tissue signal from the fundamental of the PPG signal is compared between two cases: LED duty cycle of 50% and LED duty cycle of 33%, while keeping the average activation pulse $(\overline{\Pi})$ constant. As shown in Figure 5a, the SNR of y_1 for a duty cycle of $d = 50\%$ is approximately $11.81dB$. An improvement of approximately $2.3dB$ is achieved when switching to $1.5\times$ higher LED activation pulse amplitude and a duty cycle of $d = 33\%$, which aligns with the expectations from Equation 5, and Figure 3. The noise floor remains roughly the same between these two cases but the peak of the tissue signal improves from $-103.47dB$ to $-101.17dB$.

In Figure 5b, only the LED activation signal with $d = 33\%$ is simulated, and the SNR of the extracted tissue signal (y_1) from f_c is compared to the SNR of the averaged extracted

tissue signal (y_{avg}) from f_c and $2f_c$ in the PPG signal. As shown in Figure 5 b, by averaging two copies of the signal located at the fundamental and the 2nd harmonic in the simulated PPG signal, the peak of the tissue signal slightly decreases (approximately $1.91\,dB$), while the noise power decreases by half ($3dB$). The decrease in the noise floor is greater than the decrease in the peak, resulting in an increase in the overall SNR of y_{avg} by $1.09dB$ which aligns with the expectation from Equation 8 when $M = 2$.

These simulated examples demonstrate the potential of the BASS algorithm where an overall SNR improvement of approximately $3.39dB$ was achieved by using an LED activation pulse with $d = 33\%$ and averaging the extracted tissue signal from f_c and $2f_c$ compared to the conventional method of activating the LED using a pulse signal with $d = 50\%$ and extracting the tissue signal only from f_c. This improvement in SNR is achieved without exceeding the baseline case's threshold for average emitted optical power (P_E).

6 SNR OPTIMIZATION

In this section, we formulate the design space of the extracted tissue signal as a multi-objective optimization problem based on the BASS algorithm. The problem arises from the limitation on the optical power that can be emitted on the skin from the light source, which directly affects the detected PPG signal. In this case, we assume that the heat from the LED is proportional to the optical power emitted by the light source.

The objective would be to maximize the SNR of the averaged extracted tissue signal (y_{avg}) while staying below a specific budget for the emitted optical power, as shown in Equation 9. The design space parameters include P_E, which represents the average emitted optical power, d, the duty cycle of the pulse train activating the LED, and Harmonic Content M. It is important to note that the limit imposed on P_E can easily be translated to a limit on the average of the LED activation pulse $\bar{\bar{\Pi}}$.

Equation 8 was derived to calculate the SNR of the averaged extracted tissue signal for the case when d is constant. However, as discussed in Section 4.2, the Equation 8 can be used to compare the SNR of the average extracted tissue signal with different duty cycles (d_1 and d_2), as long as the average emitted optical power (P_E) is kept constant for these two cases, which implies that $\bar{\bar{\Pi}} = A_1 d_1 = A_2 d_2$. This leads to a multi-parameter optimization problem similar to those discussed in [8, 35]:

$$
\begin{aligned}
\max\ & \mathrm{SNR}(\chi) \\
\mathrm{s.t.}\ & P_E(\chi) \leq \rho \\
& \chi \in X
\end{aligned}
$$

(9)

The deep tissue optical sensing system can be configured by adjusting the design parameter (χ) within the feasible design space solutions (X) to achieve optimal performance while ensuring that the heat generated on the skin remains within acceptable limits ($P_E \leq \rho$). The design space is as follows:

- **LED activation pulse amplitude** (A) **or LED forward current** (I_{FD}): This parameter is controlled by the LED driver and for LED activation pulse, A corresponds to the forward current (I_{FD}). The peak emitted optical power (P) is determined by I_{FD} and can be obtained from the LED's datasheet. Increasing A can enhance the SNR of the tissue signal, but it also leads to an increase in P_E resulting in higher heat generation on the skin.

- **The pulse train duty cycle** d: This parameter defines the ratio of the LED pulse on time to the LED pulse duration. The duty cycle affects both the SNR and the average emitted power, as discussed earlier. Increasing d can improve the system performance, but it also raises P_E and subsequently increases heat generation on the skin.

- **Harmonic content number** M: This parameter determines the number of PPG signal harmonics from which the tissue signal is extracted to calculate the average tissue signal y_{avg}. This parameter does NOT affect the heat output but helps reduce the system's noise floor.

By maintaining a constant P_E at the limit $P_E = \rho$, the relationship between A and d can be determined as $\bar{\bar{\Pi}} = Ad = const$, because P_E is a linear function of $\bar{\bar{\Pi}}$. As a result, the design space effectively becomes two-dimensional for exploration. Any design parameter, such as $\chi = (d, M)$ is a possible solution if it's feasible and the objective is to find optimal solutions that maximize the SNR while adhering to the power constraint imposed by the light source.

Here the average emitted optical power P_E is fixed, and the baseline SNR is derived from the design parameter $\chi_0 = (d = 50\%, M = 1)$ which represents the conventional sensing method, where the LED is activated using a pulse train with $d = 50\%$ and only the information present on the fundamental is preserved while discarding the rest of the harmonics. it is assumed that all the emitted optical power by the LED is transmitted into the body, the response of the tissue to the input light is linear, and the loss inside the tissue is constant across the frequency spectrum. These assumptions must hold true for the baseline SNR calculation.

Figure 6 illustrates the exploration of the design space and the theoretically expected improvements for each design point $\chi = (d, M)$ compared to the baseline $\chi_0 = (d = 50\%, M = 1)$ while keeping P_E constant. As observed in Figure 6, the performance of the LED activation pulse with a duty cycle of $d = 50\%$ consistently deteriorates when the tissue signal is extracted using more harmonics than the fundamental harmonic. This makes sense looking at the Fourier coefficients of a pulse train with $d = 50\%$ duty cycle. Consequently, when utilizing the BASS algorithm, the SNR of the average tissue signal (y_{avg}) starts to degrade from $M = 2$ onwards in this case.

It's important to note that the first measurable improvement using the BASS algorithm is obtained using an LED activation pulse with $d = 33\%$ and incorporating harmonic content from both f_c and $2f_c$ (design point $\chi = (d = 33\%, M = 2)$) to extract tissue signal. This design point is expected to yield an average improvement of approximately $0.6dB$ compared to extracting the tissue signal solely from the fundamental frequency (design point

$\chi = (d = 33\%, M = 1)$). In this case, the overall SNR performance increases by approximately $2.9 dB$ compared to the baseline SNR of χ_0. It's worth noting that when using an activation pulse with $d = 33\%$, there is no advantage in averaging the extracted tissue signal from $M = 3$ harmonic contents ($f_c, 2f_c,$ and $3f_c$) as the SNR of the average signal would degrade compared to using $M = 2$ harmonic contents (f_c and $2f_c$).

As mentioned earlier, the BASS algorithm demonstrates greater effectiveness when the duty cycle is lower. The results of the design space exploration support this assertion, as it is observed that for LED activation using a pulse train with $d \leq 25\%$, there are more potential gains to be achieved by averaging extracted tissue signals from two or more harmonics. A periodic pulse function with a lower duty cycle approaches closer to a periodic impulse function, which we established as the optimal LED activation signal in Section 4.1.

Theoretically, we anticipate that the best-performing design parameter would be $\chi = (5\%, M)$ with a higher M if possible. However, certain constraints, such as the limited bandwidth of the data acquisition system, impose a maximum limit on M. In real-world data, the maximum value of M is restricted to $M < F_s/(2f_c)$, where F_s represents the sampling frequency of the data acquisition system, in order to prevent aliasing. Additionally, the dynamic nature of the system can sometimes make direct comparisons between different design parameters challenging, as we will discuss in the next section.

7 EXPERIMENTAL RESULTS

The ideas presented in this paper are validated through three experimental methods. First, a test bench experiment is conducted where a high-power LED is pulsed from the bottom into a tissue phantom that simulates the optical properties of human abdominal tissue. The PPG signal is received by an optical probe placed on top of the phantom as shown in Figure 7. The effectiveness of the techniques proposed in this paper is demonstrated using a modified TFO system, which was previously reported in our work [10]. Furthermore, the setup is validated *in vivo* using a pregnant sheep model. In this case, the optical probe is placed on the belly of a pregnant sheep to capture the reflected light from the deep lamb tissue. This experiment aims to evaluate the performance of the proposed techniques in a realistic physiological scenario. Finally, the BASS algorithm is tested on a pregnant patient during a Non-Stress Test (NST) to confirm its functionality in real-world applications involving deep tissue sensing, such as non-invasive fetal signal detection.

7.1 Test Bench Setup

The optical tissue phantom, with a thickness of 5 cm, was custom-made to mimic the optical properties (absorption and scattering) of maternal abdominal tissue in term pregnancy. The optical properties were determined using parameters obtained from [7, 14]. The TFO system, as described in [10], was placed on top of the optical phantom, and an LED was positioned at the bottom which was activated with a pulse train with programmable amplitude and duty cycle. In this experiment, four different duty cycles were selected: $d = 50\%, 33\%, 25\%,$ and 20%. The amplitude of the activation pulse was adjusted inversely proportional to the duty cycle to maintain a constant average activation pulse. Consequently,

the forward current of the LED was set to $A = 200\,mA, 300\,mA, 400\,mA$, and $500\,mA$ for each respective duty cycle. The measurements were conducted for approximately 10 minutes, and the output of the photo-detector was sampled using a data acquisition system with a sampling frequency of $F_s = 8\,kSps$.

As the test bench setup does not include a tissue signal, only the DC component of y_{avg} was used to calculate the SNR. However, the rest of the analysis is conducted similarly to the case where there is a pulsating signal from the deep tissue. Table 1 presents the SNR of y_{avg} for each test case. Additionally, we measured the system's noise floor as a reference when the LED was turned off. The results are provided in Table 1. The trend in the noise floor aligns with our expectations, with a reduction in noise power of approximately M times when averaging extracted signals from the first M harmonics compared to only fundamental ($M = 1$).

The SNR values in this table are relatively high and do not precisely represent the situation in deep tissue sensing, such as non-invasive fetal pulse oximetry. This is because there are no pulsating components present from the deep tissue, and the SNR calculation is based on the DC component of the light carrier injected into the phantom. As a result, the SNR values appear higher. The best result from each measurement is indicated in bold text. It can be observed that there are SNR improvements when using lower duty cycles while increasing the pulse amplitude (A) to maintain a constant P_E. Additionally, there are mostly improvements when averaging more harmonics for duty cycles of $d = 25\%$ and $d = 20\%$. The optimal design point, in this case, would be $\chi = (20\%, 3)$.

Uncorrelated Noise: The noise present at each harmonic is uncorrelated which was verified by looking at the cross-correlation of $y_i(t)$ excluding the DC which should approximate $n_i(t)$. Here an infinitesimal correlation value was observed between $n_i(t)$ and $n_j(t)$ where $i \neq j$.

7.2 Case Study on a Pregnant Sheep

The design space exploration results from the BASS technique were tested on a novel TFO system, focusing on detecting a lamb's PPG signal inside the ewe's abdomen using pregnant sheep models. The data was acquired using the modified TFO system placed on the ewe's belly, as depicted in Figure 8, by pulsating an $850\,nm$ light source located at a distance of $7\,cm$ from the light detector. Measurements were conducted at various duty cycles while maintaining a fixed current, with each measurement lasting for 5 minutes. In this experiment, the deep tissue of interest was the fetal tissue located approximately $2\,cm$ deep from the maternal skin., and the signal of interest was the fetal heart rate signal, which was externally measured at approximately $3.02\,Hz$ or 185 beats-per-minute (bpm). The lamb's signal is indicated by the red box in Figure 9, while the remaining peaks are related to the ewe's physiological system. The noise floor was recorded when the LED was not activated, as previously mentioned. It is important to note that all procedures used in this study were evaluated and approved by the UC Davis Institutional Animal Care and Use Committee (IACUC).

Due to limitations in this experiment, the pulse amplitude was not adjusted to maintain the same average emitted optical power (P_E) while varying the duty cycle. As a result, when the duty cycle was decreased, the effective P_E also decreased. Consequently, there was a decrease in the extracted tissue signal power as the duty cycle increased, without compensating for the change in pulse amplitude. The data in Table 2 is reported as if the LED activation pulse amplitude was adjusted to account for the reduction in duty cycle. Therefore, when comparing the measurements to the baseline with a duty cycle of $d = 50\%$, the SNR values highlighted with $\star$ are adjusted in post-processing to consider the increase in the LED activation pulse amplitude by $20\log(0.50/d)\,\text{dB}$ for other duty cycles. This adjustment is made under the assumption of a constant tissue attenuation multiplier.

Here, the optimal design parameter is $\chi = (10\%, 5)$, followed by the expected optimal design parameter $\chi = (5\%, 5)$. If the system's bandwidth allowed, capturing more harmonics of the PPG signal would have further improved the SNR of the average extracted tissue signal. The trend observed in this study mostly aligns with the theoretical analysis pattern depicted in Figure 6, except for the optimal design parameter. This inconsistency can be attributed to the dynamic nature of the experiment, where the lamb is active. In such conditions, the lamb's signal and dynamics vary, leading to deviations from the expected results. In a stable condition, where the lamb's signal and dynamics remain relatively constant, the results would follow expectations more closely. Unfortunately, in the next case study, the unstable dynamics of the physiological system also persist.

7.3 Case Study on a Pregnant Patient

This protocol was approved by the UC Davis Institutional Review Board (IRB) to test this novel system in conjunction with the Non-Stress Test (NST) during antenatal visits of the pregnant patients participating in the study. Furthermore, the skin temperatures of the patients were closely monitored to ensure that increasing A and reducing d would not result in excessive heat emitted from the LEDs.

This setup was tested in experiments designed to evaluate non-invasive fetal oximetry in pregnant women, similar to the study conducted in [18]. The TFO system was placed on the pregnant mother's belly, as shown in Figure 10, to detect the reflected light from the deep fetal tissue. In this case, the tissue signal was defined as the signal present at approximately $2 - 2.5\,Hz$, corresponding to the fetus's heart rate in this experiment ($120 - 150$bpm). The main focus of this experiment was to study the effect of increasing the Harmonic Content M and observe the SNR improvement obtained by averaging multiple copies of the tissue signal. The average emitted optical power P_E was kept constant throughout the experiments. For these measurements, duty cycles of $d = 50\%, d = 33\%$, and $d = 25\%$ were selected, with pulse amplitudes of $A = 400mA, 600mA$, and $800mA$ respectively, to drive the high-power LED with a wavelength of $\lambda = 850nm$ mounted on the optical probe, and the photo-detector was positioned 4.5cm away from the source. Each measurement took approximately 2 minutes to capture, and the nature of these measurements was highly unpredictable, as the mother moved around and the fetus exhibited high activity levels.

We considered the noise floor to be constant across the experiments and used the average noise floor obtained from the three experiments, as reported in Table 3. It is important to note that the human experiment had an inherently higher noise floor compared to the animal experiment due to increased motion and a more dynamic measurement environment. This is why the dark noise floor from the previous case studies was not utilized in the SNR calculation for this case study. As observed in Table 3, it is challenging to draw a direct conclusion regarding the optimal setup when lowering the duty cycle. The dynamic nature of the system, with fast changes in the fetus' location, can result in a lower fetal signal at times, as observed in the case of $d = 33\%$. This implies that the SNR of y_1 SNR does not precisely follow the pattern depicted in Figure 3 when $M = 1$ and the duty cycle is changed. Additionally, it should be noted that the patient in the experiment was moving, which influenced the readings obtained from the TFO device. In an ideal scenario where the patient is completely stationary and measurements are taken simultaneously, we would expect an improvement in SNR from $d = 50\%$ to $d = 25\%$ that aligns with Equation 5, resulting in approximately a 3dB improvement.

However, when we shift our focus to the SNR improvement for the average extracted tissue signal (y_{avg}) at different duty cycles, we observe a pattern in the human data that aligns well with the results from the test bench and animal experiments. Figure 11 illustrates the change in SNR resulting from averaging more harmonic content for different duty cycles individually. Each data point in this figure represents the SNR difference between the design parameters $\chi = (d, M)$ and $\chi = (d, 1)$, where d represents the duty cycle and M represents the total averaged harmonic content. For example, in the case where $d = 25\%$, the optimal design point is achieved at $M = 3$, where the drop in the noise floor is more compared to the drop in the peak of the average extracted signal compared to $M = 1$ as expected. These observations provide further evidence of the effectiveness of the BASS algorithm. By conducting more measurements, we can continue to demonstrate the efficacy of the BASS algorithm and further validate its performance.

8 DISCUSSION AND FUTURE WORK

The results presented in this paper were obtained using an LED with a wavelength of $\lambda = 850nm$ based on its favorable penetration and absorption properties, which make it suitable for deep tissue signal sensing [23]. However, depending on the specific requirements of the application, a different peak wavelength for the light source can be chosen. It is important to note that the discussions and findings in this paper remain applicable and valid for the selected wavelength corresponding to the specific requirements of the deep tissue application. The validation of this algorithm involved conducting experiments at different time intervals, with slight modifications to the hardware used in each experiment. The sheep experiment was conducted prior to the human study, and at that time, the system did not reliably support increasing LED power. Despite these challenges, diligent efforts were made to test various duty cycles within a short timeframe for each study, aiming to provide multiple samples and scenarios to validate the BASS algorithm.

The test bench setup represents an ideal scenario and clearly demonstrates that the experimental results align with the expectations set by the BASS algorithm. However, it is essential to note that the stability of the physiological system was not consistent in both empirical case studies, particularly during the human study, where significant maternal motion was observed. To mitigate environmental turbulence and improve the reliability of the optical sensing system, various measures can be implemented. For example, incorporating motion reduction techniques and additional sensors can help reduce turbulence. Additionally, using accelerometers to detect motion and vibration artifacts, along with adaptive filtering techniques, can be explored to mitigate their impact on the data. Furthermore, employing multiple detectors and utilizing simultaneous information captured from different locations can enhance confidence in deep tissue signal acquisition. These strategies can help overcome the challenges posed by the dynamic nature of the physiological system and improve the robustness of the optical sensing system.

In future work, it would be interesting to investigate the optimization of harmonic selection in a broader sense. This would involve selecting harmonics with a weight assigned to them, considering all harmonics captured within the data acquisition bandwidth, rather than being limited to the summation of the first M harmonics of the fundamental, as discussed in the BASS algorithm presented in this paper. This approach resembles the feature selection problem, where the optimal number of features is selected to maximize system performance given information around each captured harmonic as a feature where the features are located at f_c and its harmonics. Machine learning methods can be explored to tackle this problem, aiming to maximize performance by utilizing time-domain or frequency-domain information extracted from each harmonic of f_c. This could potentially enhance the robustness and accuracy of the deep tissue sensing system.

9 CONCLUSION

In this paper, we have investigated the specific challenges associated with wearable optical sensing applications, particularly in the context of deep tissue sensing. The importance of optimizing the LED activation signal to maximize the SNR of the deep tissue signal is discussed while adhering to the constraints on optical power emitted onto the body. Additionally, the impact of varying the duty cycle of the LED activation pulse on the SNR of the extracted tissue signal is examined under safety considerations and limitations.

To overcome these challenges, the BASS algorithm is introduced, which employs multiple scaled copies of the tissue signal obtained from the PPG signal to enhance performance. The algorithm's effectiveness has been theoretically analyzed to evaluate its potential benefits. Furthermore, the effectiveness of this algorithm is validated through a comprehensive analysis conducted on an optical phantom in a test bench setting. Finally, *in vivo* measurements were conducted by acquiring data from both a pregnant ewe and a pregnant patient, aiming to non-invasively sense deep tissue and specifically target fetal tissue within the mother's abdomen. The effectiveness of the proposed algorithm in overcoming the SNR challenge in wearable deep tissue optical sensing applications was underscored by the findings.

ACKNOWLEDGMENT

REFERENCES

[1]. Beer. 1852. Bestimmung der Absorption des rothen Lichts in farbigen Flüssigkeiten. Annalen der Physik 162, 5 (1852), 78–88.

[2]. Beng Kok, Zahedi Edmond, and Alauddin Mohd. Ali Mohd.. 2011. Application of Adaptive Noise Cancellation in Transabdominal Fetal Heart Rate Detection Using Photoplethysmography. InTech.

[3]. Böttrich Marcel and Husar Peter. 2019. Extraction of the Fetal Pulse Curve for Transabdominal Pulse Oximetry using Adaptive and Comb Filters. In 201941 st Annual International Conference of the IEEE Engineering in Medicine and Biology Society (EMBC). 15–18. 10.1109/EMBC.2019.8856292

[4]. Böttrich Marcel, Laqua Daniel and Husar Peter. 2020. Estimating the Shape of the Fetal Pulse Curve for Transabdominal Pulse Oximetry using Synchronous Averaging. In 2020 42nd Annual International Conference of the IEEE Engineering in Medicine & Biology Society (EMBC). 1–4. 10.1109/EMBC44109.2020.9176692

[5]. International Electrotechnical Commission. 2011. IEC 60601-2-57: Medical electrical equipment —part 2–57: Particular requirements for the basic safety and essential performance of non-laser light source equipment intended for therapeutic, diagnostic, monitoring and cosmetic/aesthetic use. International Electrotechnical Commission, Tech. Rep (2011).

[6]. Fong Daniel, Knoesen André, and Ghiasi Soheil. 2017. Transabdominal fetal pulse oximetry: The case of fetal signal optimization. In 2017 IEEE 19th International Conference on e-Health Networking, Applications and Services (Healthcom). 1–6.

[7]. Fong Daniel D., Knoesen André, Motamedi Mohammad, O'Neill Terry, and Ghiasi Soheil. 2018. Recovering the fetal signal in transabdominal fetal pulse oximetry. Smart Health 9 (2018), 23–36.

[8]. Fong Daniel D., Srinivasan Vivek J., Vali Kourosh, and Ghiasi Soheil. 2019. Optode Design Space Exploration for Clinically-Robust Non-Invasive Fetal Oximetry. ACM Trans. Embed. Comput. Syst 18, 5s, Article 63 (Oct. 2019), 22 pages.

[9]. Fong Daniel D., Vali Kourosh, and Ghiasi Soheil. 2020. Contextually-aware Fetal Sensing in Transabdominal Fetal Pulse Oximetry. In 2020 ACM/IEEE 11th International Conference on Cyber-Physical Systems (ICCPS). 119–128.

[10]. Fong Daniel D., Yamashiro Kaeli J., Vali Kourosh, Galganski Laura A., Thies Jameson, Moeinzadeh Rasta, Pivetti Christopher, Knoesen André, Srinivasan Vivek J., Hedriana Herman L., Farmer Diana L., Johnson Michael Austin, and Ghiasi Soheil. 2021. Design and In Vivo Evaluation of a Non-Invasive Transabdominal Fetal Pulse Oximeter. IEEE Transactions on Biomedical Engineering 68, 1 (2021), 256–266. [PubMed: 32746021]

[11]. Glaros Konstantinos N. 2011. Low-power pulse oximetry and transimpedance amplifiers. Ph. D. Dissertation. Imperial College London. 10.25560/9480

[12]. Hobbs Philip C. D.. 2009. Building Electro-Optical Systems: Making It All Work (2nd ed.). Wiley Publishing.

[13]. Jacques Steven L. 2013. Optical properties of biological tissues: a review. Physics in Medicine Biology 58, 11 (may 2013), R37. 10.1088/0031-9155/58/11/R37 [PubMed: 23666068]

[14]. Jakubowski Dorota B., Cerussi Albert E., Bevilacqua Frédéric P., Shah Natasha, Hsiang David, Butler John A., and Tromberg Bruce J.. 2004. Monitoring neoadjuvant chemotherapy in breast cancer using quantitative diffuse optical spectroscopy: a case study. Journal of Biomedical Optics 9, 1 (2004), 230 – 238. 10.1117/1.1629681 [PubMed: 14715078]

[15]. Joarder Rishad, Kasap Begum, and Ghiasi Soheil. 2023. RT-TRAQ: An algorithm for real-time tracking of faint quasiperiodic signals in noisy time series. Smart Health 28 (2023), 100392. 10.1016/j.smhl.2023.100392 [PubMed: 37974565]

[16]. Kalvoy Havard, Martinsen Orjan G., and Grimnes Sverre. 2008. Determination of tissue type surrounding a needle tip by electrical bioimpedance. In 2008 30th Annual International Conference of the IEEE Engineering in Medicine and Biology Society. 2285–2286. 10.1109/IEMBS.2008.4649653

[17]. Kasap Begum, Vali Kourosh, Qian Weitai, Chak Wai Ho, Vafi Ata, Saito Naoki, and Ghiasi Soheil. 2021. Multi-Detector Heart Rate Extraction Method for Transabdominal Fetal Pulse Oximetry. In 2021 43rd Annual International Conference of the IEEE Engineering in Medicine Biology Society (EMBC). 1072–1075.

[18]. Kasap Begum, Vali Kourosh, Qian Weitai, Mo Lihong, Chithiwala Zahabiya H., Hedriana Herman L., and Ghiasi Soheil. 2023. Use of A Novel Transabdominal Fetal Pulse Oximeter (TFO) In Human Pregnancy: A Proof-of-Concept. American Journal of Obstetrics and Gynecology 228, 1, Supplement (2023), S100. 10.1016/j.ajog.2022.11.211 SMFM 43rd Annual Meeting: The Pregnancy Meeting.

[19]. Kasap Begum, Vali Kourosh, Qian Weitai, Saffarpour Mahya, and Ghiasi Soheil. 2023. KUBAI: Sensor Fusion for Non-Invasive Fetal Heart Rate Tracking. IEEE Transactions on Biomedical Engineering (2023), 1–10. 10.1109/TBME.2023.3238736

[20]. Lathi BP and Ding Z. 2009. Modern Digital and Analog Communication Systems. Oxford University Press. https://books.google.com/books?id=dltNPwAACAAJ

[21]. Liu Shing-Jiuan, Ghiasi Soheil, and Yang Weijian. 2021. Combined CW and FMCW near infrared spectroscopy for transabdominal fetal oximetry. In Optical Diagnostics and Sensing XXI: Toward Point-of-Care Diagnostics, Coté Gerard L. (Ed.), Vol. 11651. International Society for Optics and Photonics, SPIE, 116510M. 10.1117/12.2578810

[22]. Liu Yihan, Menon Rahul, Putcha Arjun, Huang Ke, Bonilla Leonardo, Vora Rohan, Li Junye, Zhang Lin, Wang Yihang, Fletcher Lauren, Lassiter Anna, Huang Chuqi, Buse John B., Cheng Ke, and Bai Wubin. 2022. Skin-Interfaced Deep-Tissue Sensing Patch via Microneedle Waveguides. Advanced Materials Technologies 7, 9 (2022), 2200468. 10.1002/admt.202200468

[23]. Mannheimer PD, Cascini JR, Fein ME, and Nierlich SL. 1997. Wavelength selection for low-saturation pulse oximetry. IEEE Transactions on Biomedical Engineering 44, 3 (1997), 148–158. 10.1109/10.554761 [PubMed: 9216128]

[24]. Niwayama Masatsugu and Unno Naoki. 2021. Tissue Oximeter with Selectable Measurement Depth Using Spatially Resolved Near-Infrared Spectroscopy. Sensors 21, 16 (2021). 10.3390/s21165573

[25]. Oppenheim AV. 1999. Discrete-Time Signal Processing. Pearson Education. https://books.google.com/books?id=geTn5W47KEsC

[26]. Pisa Stefano, Pittella Erika, and Piuzzi Emanuele. 2016. A survey of radar systems for medical applications. IEEE Aerospace and Electronic Systems Magazine 31, 11 (2016), 64–81. 10.1109/MAES.2016.140167

[27]. Rompelman O and Ros HH. 1986. Coherent averaging technique: A tutorial review Part 1: Noise reduction and the equivalent filter. Journal of Biomedical Engineering 8, 1 (1986), 24–29. 10.1016/0141-5425(86)90026-9 [PubMed: 3951206]

[28]. Sonmezoglu Soner, Fineman Jeffrey, Maltepe Emin, and Maharbiz MM. 2021. Monitoring deep-tissue oxygenation with a millimeter-scale ultrasonic implant. Nature Biotechnology 39 (07 2021). 10.1038/s41587-021-00866-y

[29]. Tavakoli Maziar, Turicchia Lorenzo, and Sarpeshkar Rahul. 2010. An Ultra-Low-Power Pulse Oximeter Implemented With an Energy-Efficient Transimpedance Amplifier. IEEE Transactions on Biomedical Circuits and Systems 4, 1 (2010), 27–38. 10.1109/TBCAS.2009.2033035 [PubMed: 23853307]

[30]. Vafi Ata, Vali Kourosh, Kasap Begum, Hu Jonathan C, Kurzrock Eric, and Ghiasi Soheil. 2023. Towards Non-Invasive Bladder Volume Sensing via Bio-Impedance Spectroscopy: Feasibility Demonstration in Ex-Vivo Bladder Models. In Proceedings of the ACM/IEEE 14th International Conference on Cyber-Physical Systems. 34–43. 10.1145/3576841.3585932

[31]. Vali Kourosh, Kasap Begum, Qian Weitai, Theodorou Christina M., Lihe Tailai, Fong Daniel D., Pivetti Christopher D., Kulubya Edwin S., Yamashiro Kaeli J., Wang Aijun, Johnson M. Austin, Hedriana Herman L., Farmer Diana L., and Ghiasi Soheil. 2021. 974 Non-invasive transabdominal assessment of In-Utero fetal oxygen saturation in a hypoxic lamb model. American Journal of Obstetrics and Gynecology 224, 2, Supplement (2021), S604.

[32]. Vali Kourosh, Kasap Begum, Qian Weitai, Vafi Ata, Saffarpour Mahya, and Ghiasi Soheil. 2021. Estimation of Fetal Blood Oxygen Saturation from Transabdominally Acquired Photoplethysmogram Waveforms. In 2021 43rd Annual International Conference of the IEEE Engineering in Medicine Biology Society (EMBC). 1100–1103.

[33]. Vondran David J. 2011. Extending Millimeter-wave Measurement Systems with Harmonic Mixer Technology. Microwave Journal (2011).

[34]. Wang Lihong V.. 2007. Biomedical optics : principles and imaging / Wang Lihong V., Wu Hsin-i. Wiley-Interscience, Hoboken, N.J.

[35]. Zadeh L. 1963. Optimality and non-scalar-valued performance criteria. IEEE Trans. Automat. Control 8, 1 (1963), 59–60. 10.1109/TAC.1963.1105511

[36]. Zourabian Anna, Siegel Andy, Chance Britton, Ramanujam Nirmala, Rode Martha, and Boas David A.. 2000. Transabdominal monitoring of fetal arterial blood oxygenation using pulse oximetry. Journal of Biomedical Optics 5, 4 (2000), 391–405. [PubMed: 11092427]

CCS Concepts:

• Applied computing → Life and medical sciences; • Computer systems organization → Embedded and cyber-physical systems.
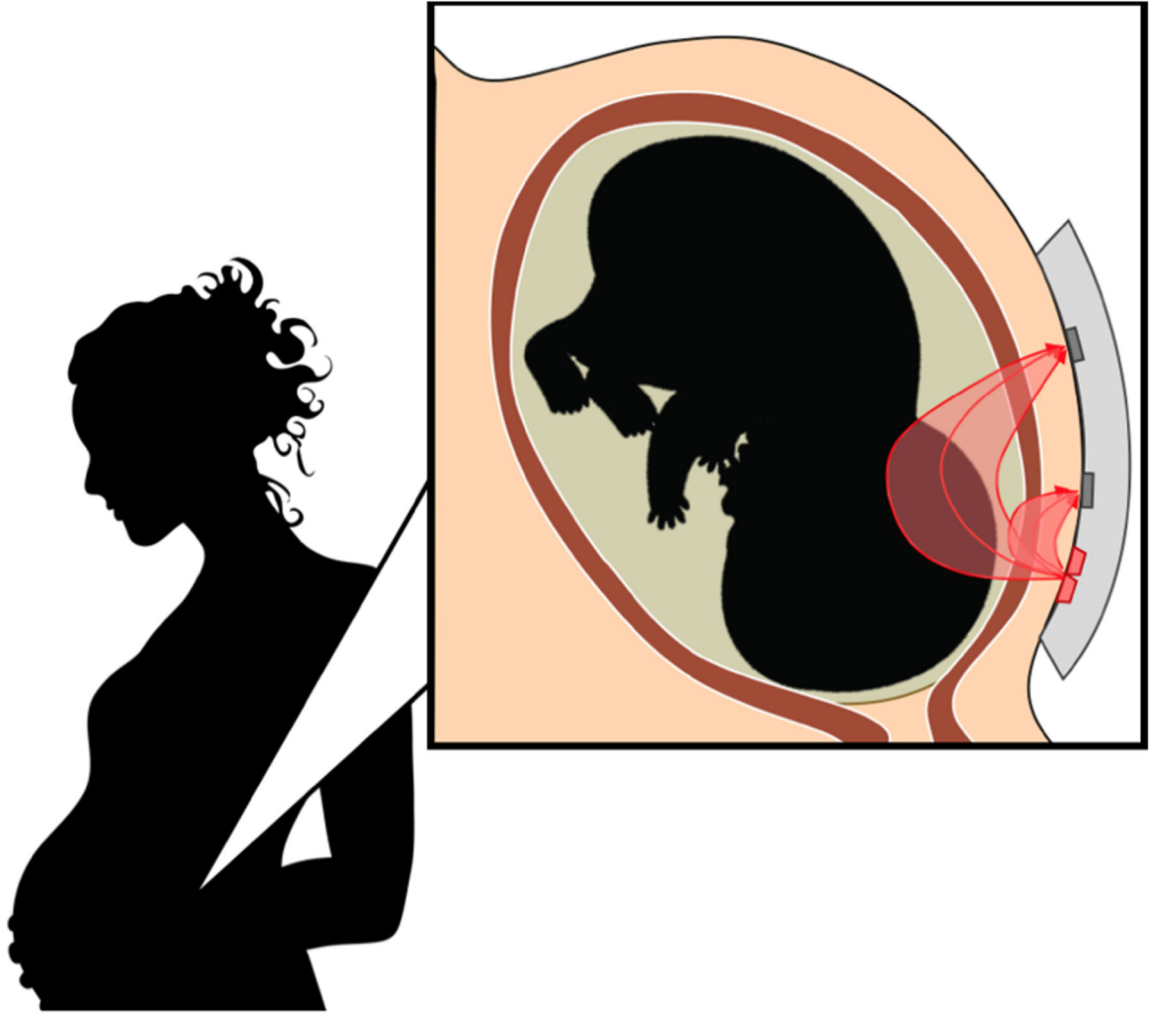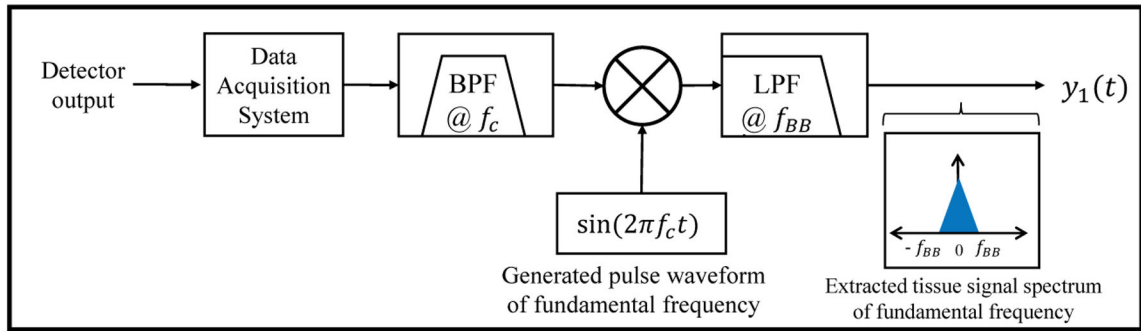
Fig. 1.
High-level overview of non-invasive fetal pulse oximetry, an illustrative application of deep tissue optical sensing [10].
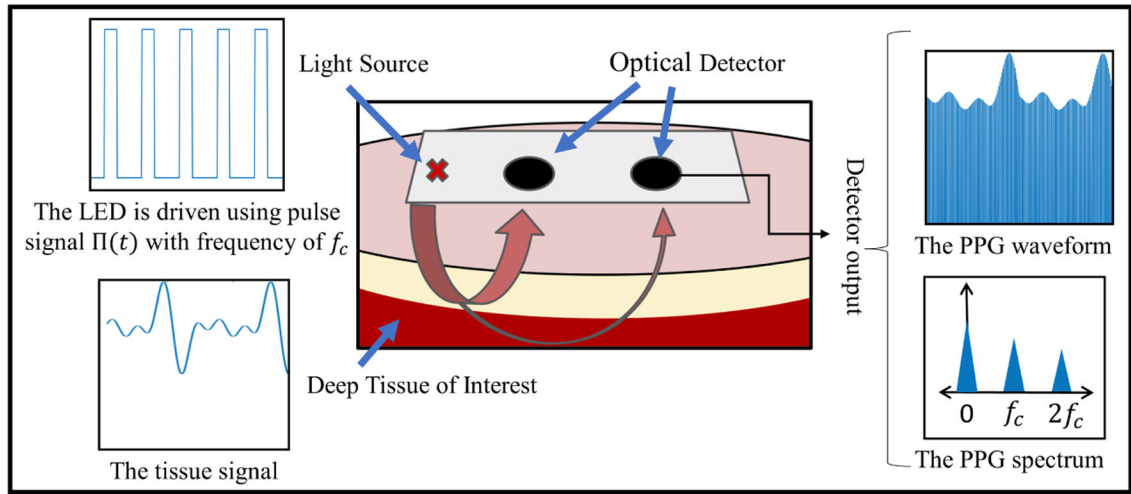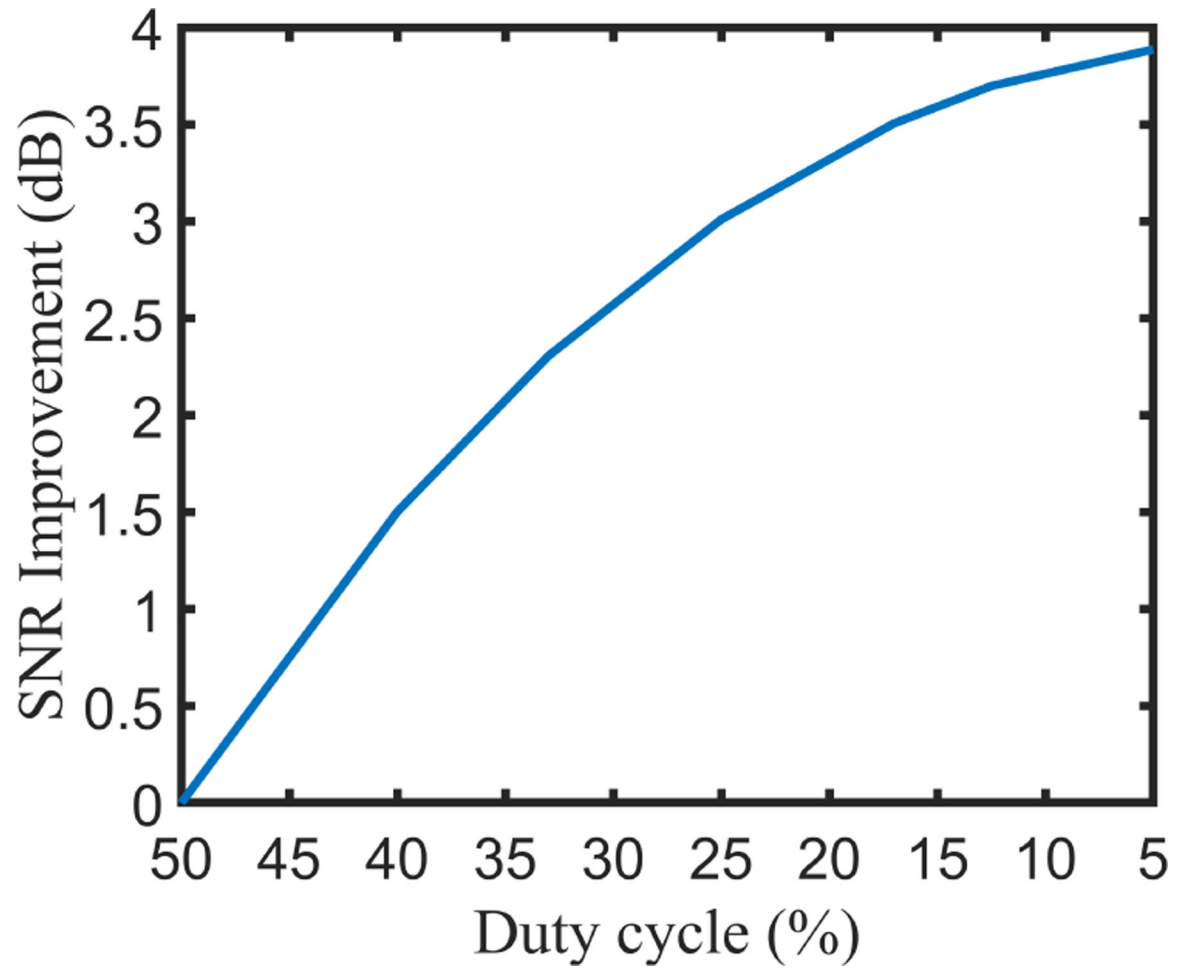
(a) The detection of the deep tissue signal by pulsating an LED on the skin.
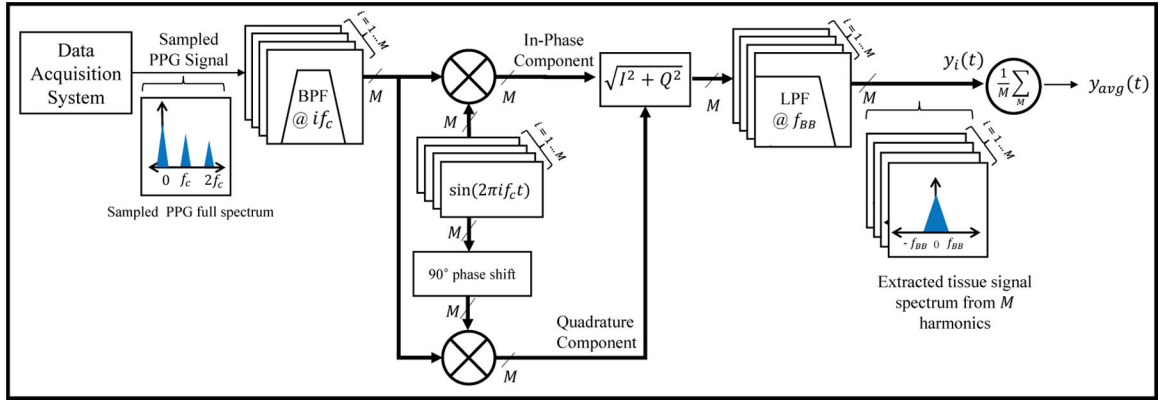

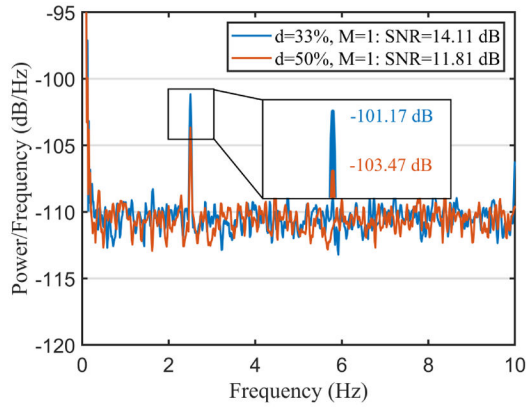(b) The extracted noisy tissue signal from the fundamental frequency of the detected PPG signal.
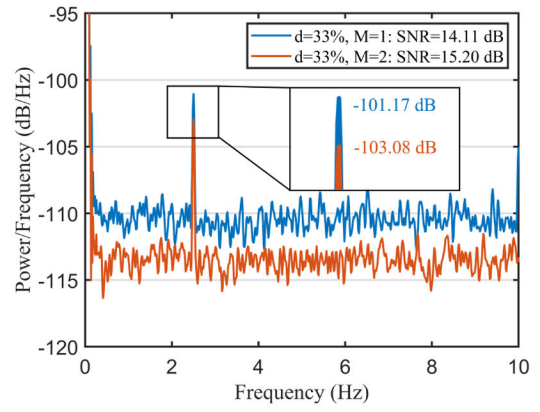
Fig. 2.
Synchronous Detection procedure

Fig. 3.
SNR improvement of y_1 for different duty cycles compared to $d = 50\%$ with constant P_E.

Fig. 4.
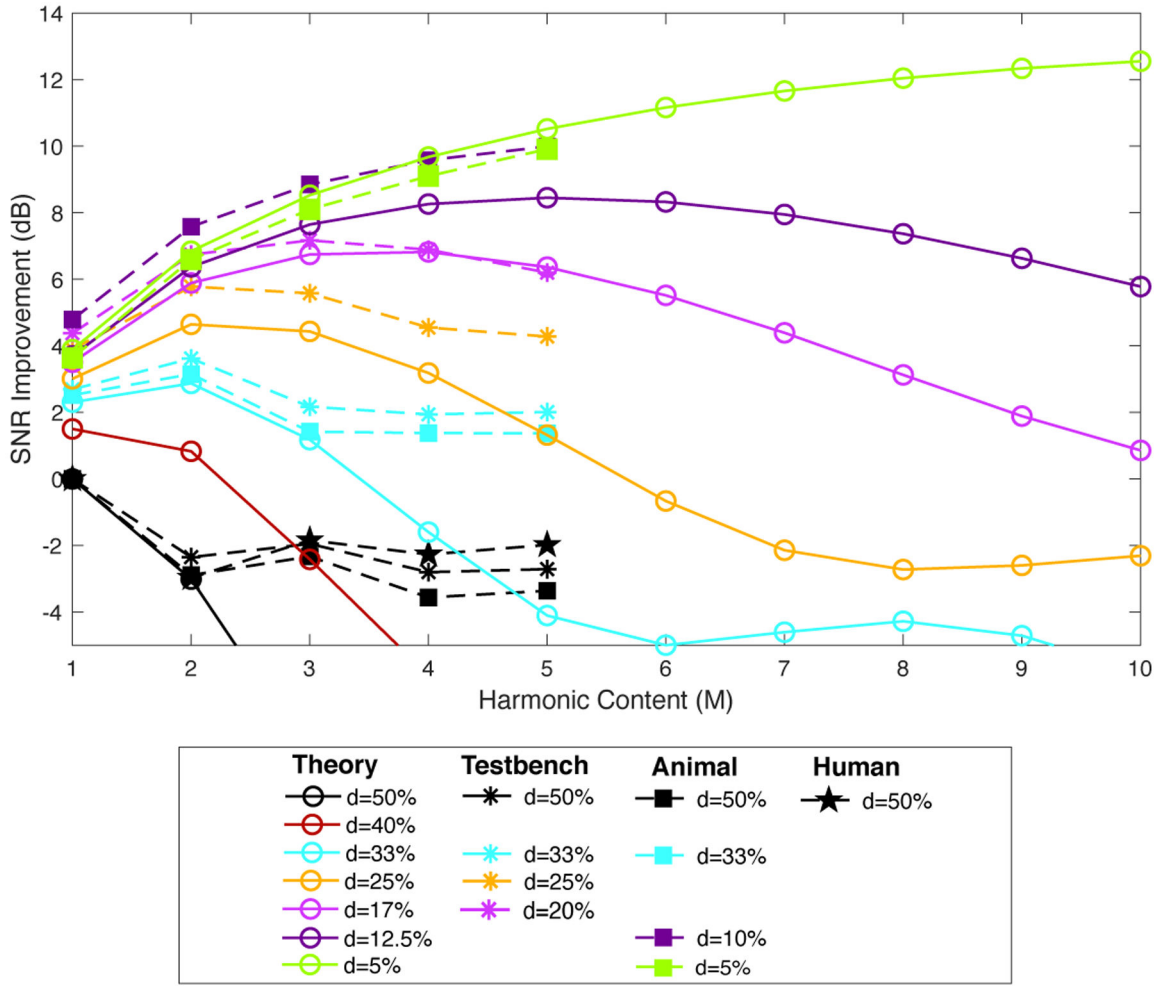The high-level BASS algorithm scheme. M indicates the depth of each filter.

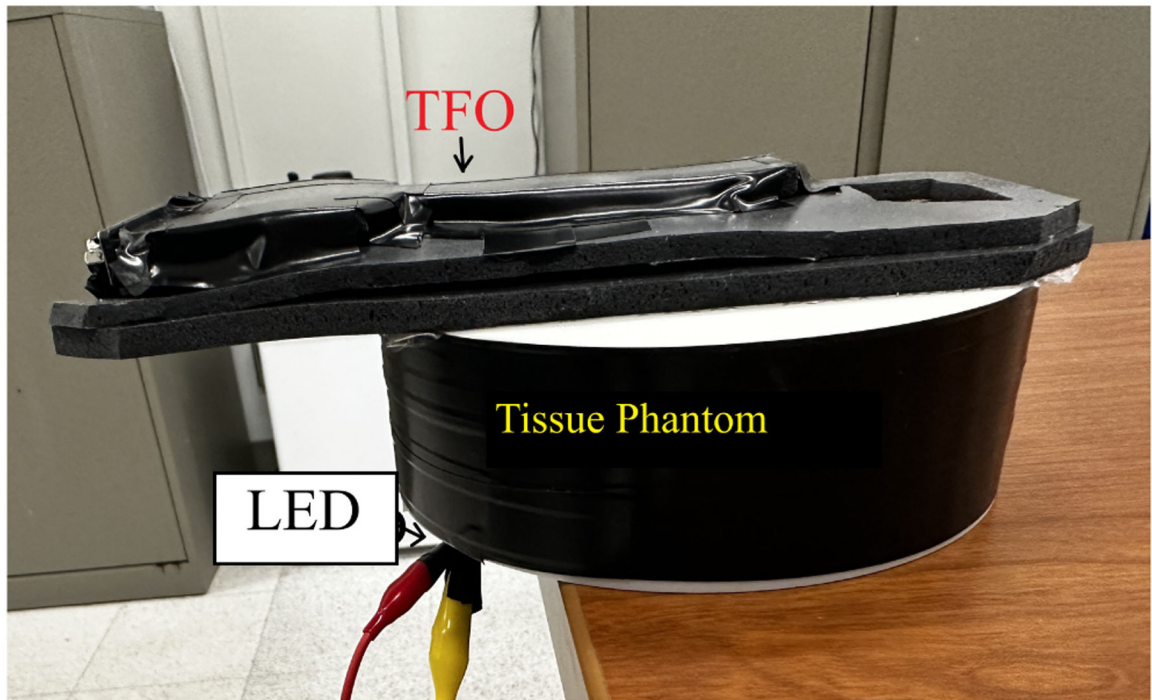(a) y_1 PSD for two cases when $d = 50\%$ vs $d = 33\%$ with constant $\overline{\Pi}$.

(b) y_{avg} PSD when $d = 33\%$ for two cases when $M = 1$ vs $M = 2$.
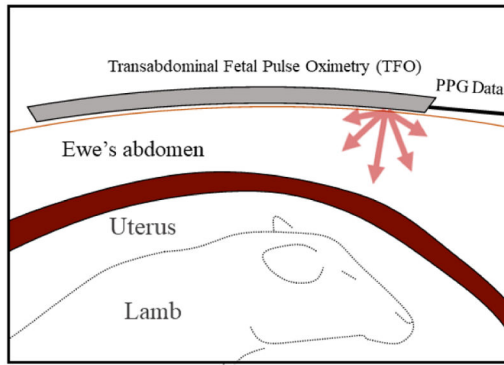
Fig. 5.
Examples of averaged extracted tissue signal PSD.

Fig. 6.
SNR improvements at each $\chi = (d, M)$ design point compared to baseline $\chi_0 = (50\%, 1)$ for theoretical and experimental results.

Fig. 7.
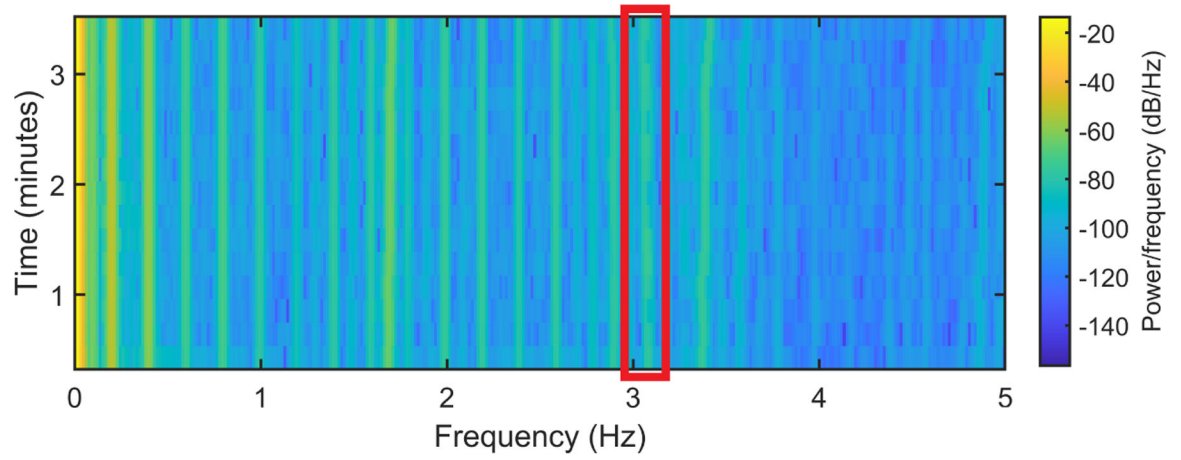The setup on a tissue phantom with LED underneath.

(a) Illustration of the study [31].

(b) TFO placement in the study.

Fig. 8.
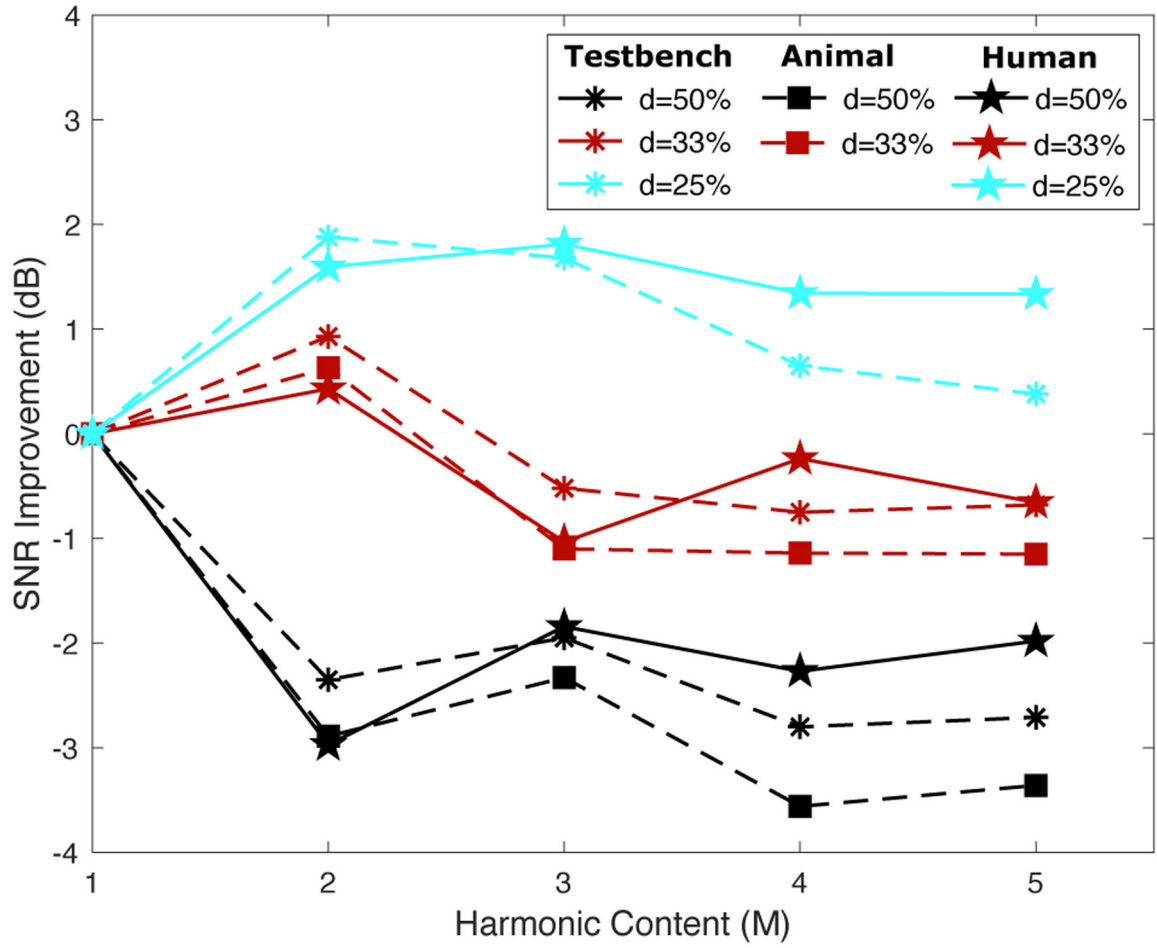Deep tissue optical sensing in a hypoxic sheep model

Fig. 9.
PPG spectrogram when *d* = 50%. Here the whereabouts of the lamb's signal are indicated with red over time.

Fig. 10.
TFO on a human experiment.

Fig. 11.
SNR improvements at each $\chi = (d, M)$ design points with respect to $\chi_0 = (d, 1)$.

Table 1.

y_{avg} SNR from test bench setup at various (d, M) where P_E is kept constant.

		Average Extracted Tissue Signal SNR				
		$M = 1$	$M = 2$	$M = 3$	$M = 4$	$M = 5$
Duty Cycle (d)	50%	**90.90dB**	88.55 dB	88.95dB	88.10dB	88.19dB
	33%	93.59dB	**94.52dB**	93.07dB	92.84dB	92.91dB
	25%	94.80dB	**96.68dB**	96.48dB	95.45dB	95.18dB
	20%	95.28dB	97.64dB	**98.07dB**	97.79dB	97.10dB
		Noise Power				
		−144.90dB	−148.05dB	−149.76dB	−151.04dB	−152.14dB

Table 2.

y_{avg} SNR in a sheep model at various (d, M) for activation pulse.

		Average Extracted Tissue Signal SNR				
		$M = 1$	$M = 2$	$M = 3$	$M = 4$	$M = 5$
Duty Cycle	50%	**53.72dB**	50.83dB	51.39dB	50.16dB	50.36dB
	33%★	56.24dB	**56.87dB**	55.14dB	55.10dB	55.09dB
	10%★	58.51dB	61.30dB	62.57dB	63.30dB	**63.71dB**
	5%★	57.36dB	60.31dB	61.82dB	62.85dB	**63.63dB**

Table 3.

y_{avg} SNR and noise power in an experiment on a pregnant patient.

		Average Extracted Tissue Signal SNR				
		$M = 1$	$M = 2$	$M = 3$	$M = 4$	$M = 5$
Duty cycle(d)	50%	**11.28dB**	8.31dB	9.44dB	9.01dB	9.30dB
	33%	0.04dB	**0.46dB**	−0.98dB	−0.20dB	−0.62dB
	25%	9.78dB	11.38dB	**11.59dB**	11.12dB	11.11dB
		Noise Power				
		−99.76dB	−102.77dB	−105.08dB	−107.15dB	−108.36dB